Green Chemical Technology

SCIEPublish

Article

Lanthanum-Modified Activated Alumina for Selective Removal of Fluoride from Phosphogypsum Leachate

Shuomin Hou [1], Zhaobo Wang [1,*], Xiang Peng [2,*], Shengchao Huang [3], Huijuan Ma [3] and Ruan Chi [1,4]

[1] Phosphogypsum Utilization R&D Center, Hubei Three Gorges Laboratory, Yichang 443007, China; houshuomin@hbsxsys.com (S.H.); rac@wit.edu.cn (R.C.)
[2] State Key Laboratory of Green and Efficient Development of Phosphorus Resources, Hubei Key Laboratory of Plasma Chemistry and Advanced Materials, Wuhan Institute of Technology, Wuhan 430205, China
[3] Hubei Xingfa Chemicals Group Co., Ltd., Yichang 443007, China; huangshengchao@xfjt.com (S.H.); MHJ19831225@163.com (H.M.)
[4] Shool of Resources and Safety Engineering, Wuhan Insititute of Technology, Wuhan 430073, China

* Corresponding author. E-mail: wangzhaobo@hbsxsys.com (Z.W.); xpeng@wit.edu.cn (X.P.)

Received: 4 June 2026; Revised: 23 June 2026; Accepted: 16 July 2026; Available online: 24 July 2026

ABSTRACT: Fluoride-rich phosphogypsum leachate is a challenging industrial wastewater because of its low pH, high ionic strength, and the presence of competing anions. In this study, lanthanum-modified activated alumina (La-AA) was prepared and evaluated as a selective adsorbent for the removal of fluoride from complex phosphate-industry wastewater. The results showed that La modification improved the adsorption performance of activated alumina, and the 10% La-AA sample exhibited the best fluoride removal behavior among the tested materials. Kinetic and thermodynamic analyses indicated that fluoride adsorption on La-AA was more favorable than on pristine activated alumina and proceeded spontaneously and endothermically under the tested conditions. In competitive adsorption tests, La-AA maintained better fluoride uptake than unmodified activated alumina in the presence of chloride, sulfate, and phosphate, demonstrating improved matrix tolerance. When applied to authentic phosphogypsum leachate, the optimized La-AA reduced fluoride concentration from 9.67 $mg \cdot L^{-1}$ to 0.58 $mg \cdot L^{-1}$, below the WHO guideline value. These results suggest that La modification is a practical strategy to improve the selectivity and applicability of activated alumina for fluoride removal in complex industrial process water.

Keywords: Activated alumina; Lanthanum modification; Selective removal; Fluoride adsorption; Phosphogypsum leachate

1. Introduction

The management of fluoride-containing wastewater remains a significant challenge in phosphate-related mineral processing and chemical production. While fluoride is an essential trace element, prolonged exposure to high concentrations can cause severe health disorders, including dental and skeletal fluorosis, neurological damage, and compromised thyroid function. The World Health Organization (WHO) sets the

maximum permissible concentration of fluoride in drinking water at 1.5 $mg \cdot L^{-1}$ [1,2]. This problem is particularly acute in regions associated with geological fluoride enrichment or intensive industrial activity, such as phosphate fertilizer production [3].

The treatment of fluoride-contaminated water, especially industrial wastewater, is notoriously difficult. Adsorption is a favored technique due to its operational simplicity and cost-effectiveness, with activated alumina (AA) being one of the most historically employed adsorbents [4–7]. Its mechanism primarily involves ligand exchange between surface hydroxyl groups (≡Al–OH) and F^- ions [8–12]. However, conventional AA suffers from critical limitations that undermine its practical utility: (1) modest adsorption capacity [13,14], (2) significant performance deterioration under acidic conditions [15,16], and most critically, (3) poor selectivity in the presence of competing anions [17]. Co-existing oxyanions such as phosphate (PO_4^{3-}) and sulfate (SO_4^{2-}), common in industrial effluents, exhibit a strong affinity for aluminum sites, leading to severe competition for adsorption sites and drastically reduced fluoride removal efficiency [18]. This intrinsic lack of selectivity represents the central bottleneck in applying adsorption technologies to real-world, complex wastewater streams.

To overcome this bottleneck, engineering the adsorbent surface to possess preferential affinity for fluoride is paramount. In this context, modification with multivalent metal cations has emerged as a promising strategy [18–24]. Among these, La^{3+} stands out due to its strong Lewis acidity, high affinity for fluoride ions (forming stable La–F bonds), and relatively low environmental impact [25,26]. Recent studies have shown that La-impregnated materials can enhance fluoride uptake capacity [26,27]. However, the prevailing literature predominantly focuses on performance in synthetic, single-analyte systems. A critical research gap persists in the fundamental understanding of how La modification alters the adsorption mechanism, particularly the kinetics and thermodynamics. More importantly, whether this translates into genuine selectivity and robustness in chemically complex, real-world wastewater is still missing. Demonstrating efficacy in such matrices is the true litmus test for any proposed adsorbent.

Phosphogypsum leachate presents an ideal, stringent case study to address this gap. Generated from the stockpiling of phosphogypsum (a byproduct of phosphate fertilizer manufacturing), phosphogypsum leachate is characterized by extreme acidity, high ionic strength, and exceptionally high concentrations of fluoride alongside overwhelming amounts of competing ions like phosphate and sulfate [28]. It therefore epitomizes the "complex wastewater matrix" where traditional adsorbents like AA fail.

Herein, La-modified activated alumina (La-AA) was developed to improve fluoride adsorption performance and, more importantly, to enhance selectivity toward fluoride in the presence of competing anions. The resulting adsorbents were systematically synthesized and characterized, and their adsorption behavior was compared with that of pristine activated alumina in terms of kinetics, isotherms, and thermodynamics. In addition, the selectivity of La-AA was evaluated in the presence of representative coexisting anions, and its practical applicability was further assessed using authentic high-strength phosphogypsum leachate. This study, therefore, provides both mechanistic insight into the role of La modification in selective fluoride adsorption and experimental evidence supporting its use in treating complex phosphate-industry wastewater.

2. Materials and Methods

2.1. Materials and Reagents

Activated alumina (AA) and lanthanum (III) nitrate hexahydrate ($La(NO_3)_3 \cdot 6H_2O$) were purchased from Energy Chemical. Sodium fluoride (NaF), sodium chloride (NaCl), sodium dihydrogen phosphate dihydrate ($NaH_2PO_4 \cdot 2H_2O$), and sodium sulfate (Na_2SO_4) were obtained from Aladdin. Nitric acid (HNO_3) was procured from Xilong Scientific. All solutions were prepared using deionized water (DW). The raw phosphogypsum leachate was provided by a phosphate chemical plant in Hubei Province, China.

2.2. Materials Preparation

La-AA was prepared by an alkali-assisted impregnation method. Briefly, 50 g of AA was dispersed in 500 mL of 0.15 M NaOH solution and stirred for 1 h at room temperature. The resulting solid was filtered, thoroughly washed with DW, and dried at 105 °C for 12 h. Subsequently, 5 g of the NaOH-treated AA was added to 100 mL of $La(NO_3)_3 \cdot 6H_2O$ solutions with nominal concentrations of 2.5, 5, 7.5, 10, and 12.5 wt%, respectively. The suspensions were impregnated for 12 h. The solids were then filtered and dried at 105 °C for 12 h. The obtained samples were denoted as x% La-AA, where x represents the nominal La impregnation concentration.

2.3. Materials Characterization

The phase identification was performed by X-ray diffraction using a Rigaku D/MAX-2500V/PC diffractometer (Rigaku, Tokyo, Japan). The surface morphology and elemental composition of the adsorbents were examined using a Thermo Scientific Helios 5 UC scanning electron microscope (SEM) equipped with an energy-dispersive X-ray spectroscopy (EDS) detector (Thermo Fisher Scientific, Waltham, MA, USA). The specific surface area, pore volume, and pore size distribution were determined by nitrogen adsorption-desorption measurements at 77 K using a Micromeritics ASAP 2460 analyzer (Micromeritics Instrument Corporation, Norcross, GA, USA). The Brunauer-Emmett-Teller (BET) method was used to calculate the specific surface area, and the Barrett-Joyner-Halenda (BJH) method was used to determine pore size parameters. X-ray photoelectron spectroscopy (XPS) was conducted on a Thermo Scientific EscaLab Xi+ electron spectrometer (Thermo Fisher Scientific, Waltham, MA, USA) using Al Kα radiation (200 W). The binding energy was calibrated using the C 1s peak at 284.8 eV.

2.4. Adsorption Experiments

The fluoride concentration in solution was measured using a METTLER TOLEDO Seven Direct SD50 fluoride ion meter (Mettler-Toledo International Inc., Greifensee, Switzerland). All batch experiments were carried out in 50 mL centrifuge tubes on an orbital shaker at 200 rpm. After adsorption, the suspensions were filtered through 0.45 μm membrane filters, and the fluoride concentration in the filtrate was analyzed.

For adsorption kinetics, 0.1 g of adsorbent (AA or 10% La-AA) was added to 40 mL of 100 $mg \cdot L^{-1}$ fluoride solution. The suspension was shaken at room temperature (25 °C), and samples were collected at 5, 10, 20, 30, 40, 60, 90, and 120 min.

For adsorption isotherms and thermodynamic analysis, 0.05 g of adsorbent was added to 40 mL of fluoride solutions with initial concentrations ranging from 25 to 300 $mg \cdot L^{-1}$ at pH 4. The experiments were performed at 25, 35, and 45 °C [29].

To evaluate the effects of key operating parameters, the influence of La loading (0–12.5%), solution pH (2–10), adsorbent dosage (0.05–0.25 g in 40 mL of 100 $mg \cdot L^{-1}$ fluoride solution), initial fluoride concentration (25–300 $mg \cdot L^{-1}$ at pH 4), and temperature (25–85 °C for 25 $mg \cdot L^{-1}$ fluoride solution) was investigated. The contact time was 1 h unless otherwise specified.

For competitive adsorption tests, solutions containing 25 $mg \cdot L^{-1}$ fluoride and a tenfold molar excess of competing anions (Cl^-, SO_4^{2-}, or PO_4^{3-}) were prepared at pH 4. Then, 0.05 g of adsorbent was added to 40 mL of each solution and shaken at 55 °C for 1 h.

For the treatment of real phosphogypsum leachate, the raw leachate was diluted 100-fold with deionized water. Different dosages (0.1–1.0 g) of 10% La-AA were then added to 40 mL of the diluted leachate and shaken at 70 °C for 1 h.

2.5. Data Analysis

The adsorption capacity at equilibrium, q_e ($mg \cdot g^{-1}$), was calculated using Equation (1):

$$q_e = \frac{(C_0 - C_e)V}{M} \quad (1)$$

where C_0 and C_e (mg·L^{-1}) are the initial and equilibrium F^- concentrations, respectively; V (L) is the solution volume, and M (g) is the mass of the adsorbent. The removal efficiency (%) was calculated as ($C_0 - C_e$)/C_0 × 100%.

Adsorption kinetics data were fitted using the pseudo-first-order (PFO, Equation (2)) and pseudo-second-order (PSO, Equation (3)) models.

$$q_t = q_e\left(1 - e^{-k_1 t}\right) \quad (2)$$

$$q_t = \frac{k_2 q_e^{\,2} t}{1 + k_2 q_e t} \quad (3)$$

where q_t (mg·g^{-1}) is the adsorption capacities at time t; k_1 (min^{-1}) and k_2 (g·mg^{-1}·min^{-1}) are the rate constants.

Adsorption isotherms were analyzed using the Langmuir (Equation (4)) and the Freundlich (Equation (5)) models.

$$q_e = \frac{Q_m K_L C_e}{1 + K_L C_e} \quad (4)$$

$$q_e = K_F C_e^{\frac{1}{n}} \quad (5)$$

where Q_m (mg·g^{-1}) is the theoretical maximum adsorption capacity; K_L (L·mg^{-1}) is the Langmuir constant related to adsorption energy; K_F ((mg·g^{-1})(L·mg^{-1})$^{1/n}$) and n are the Freundlich constants indicating adsorption capacity and intensity, respectively.

Thermodynamic parameters, including Gibbs free energy change (ΔG^0), enthalpy change (ΔH^0), and entropy change (ΔS^0), were calculated from the temperature-dependent isotherm data using Equations (6)–(8).

$$\Delta G^0 = -RT\ln K_0 \quad (6)$$

$$\ln K_0 = \frac{\Delta S^0}{R} - \frac{\Delta H^0}{RT} \quad (7)$$

$$\Delta S = \frac{\Delta H - \Delta G}{T} \quad (8)$$

where K_0 is the distribution coefficient, R (8.314 J·(mol·K)$^{-1}$) is the ideal gas constant, and T (K) is the absolute temperature. ΔH^0 (KJ·mol^{-1}) and ΔS^0 (J·(mol·K)$^{-1}$) were obtained from the slope and intercept of the linear plot of lnK_0 *vs*. 1/T.

3. Results and Discussion

3.1. Materials Characterization

The morphology and textural properties of the adsorbents were examined to verify successful modification and to clarify the structural basis for fluoride adsorption. Figure 1 presented the XRD patterns of activated alumina before and after La modification. It was found that no obvious changes were observed in the characteristic diffraction peaks after La doping. SEM images (Figure 2a–g) show that both pristine

AA and La-AA samples consist of irregular granular particles with sizes around 50 μm. No significant morphological change was observed after NaOH treatment or La impregnation, indicating that the modification process did not alter the overall particle structure. EDS analysis (Figure 3 and Table 1) confirmed the successful loading of La onto the AA surface. The actual La content increased from 3.01 wt.% to 5.58 wt.% as the nominal impregnation concentration rose from 2.5% to 12.5%. A sharp increment was observed within the La loading range of 2.5–10%. Further raising the nominal La loading from 10% to 12.5% only led to a 0.38 wt% rise in real La content, matching the trend of fluoride uptake.

Table 1. Elemental composition (wt.%) of samples from EDS analysis.

Samples	Elemental Content		
	Al (wt.%)	O (wt.%)	La (wt.%)
AA	38.77	61.23	/
NaOH-AA	48.33	51.67	/
2.5% La-AA	47.70	49.28	3.01
5% La-AA	49.20	47.47	3.33
7.5% La-AA	47.56	47.77	4.67
10% La-AA	47.18	47.62	5.20
12.5% La-AA	47.40	47.02	5.58

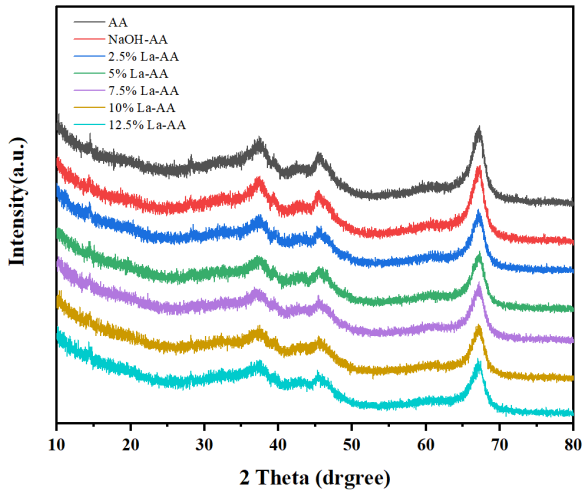

Figure 1. XRD patterns of activated alumina before and after La modification.

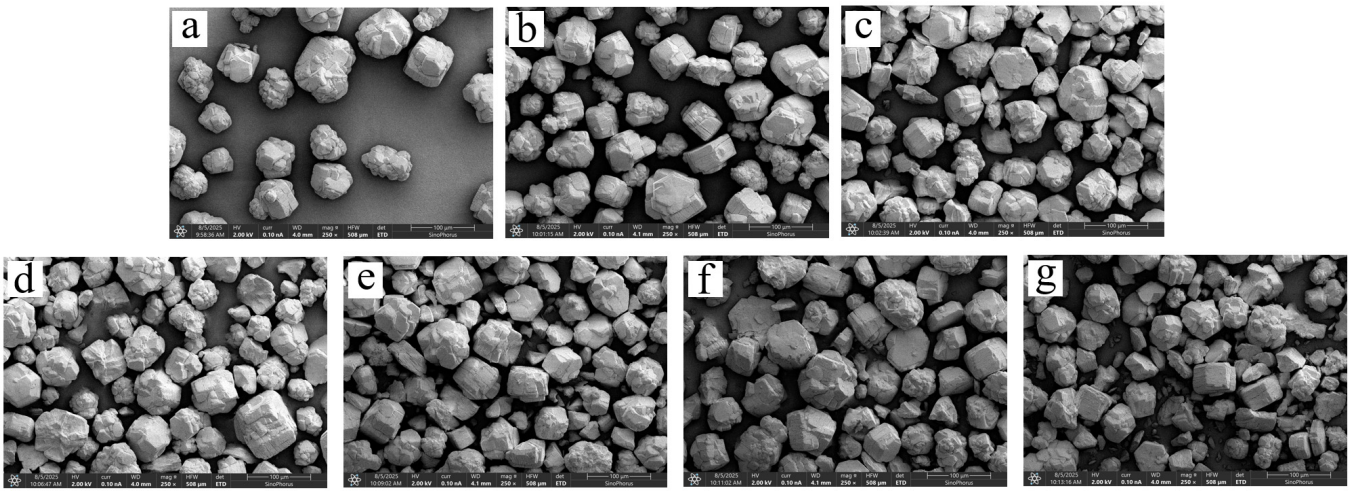

Figure 2. SEM of samples: (**a**) AA, (**b**) NaOH-AA, (**c**) 2.5% La-AA, (**d**) 5% La-AA, (**e**) 7.5% La-AA, (**f**) 10% La-AA, and (**g**) 12.5% La-AA.

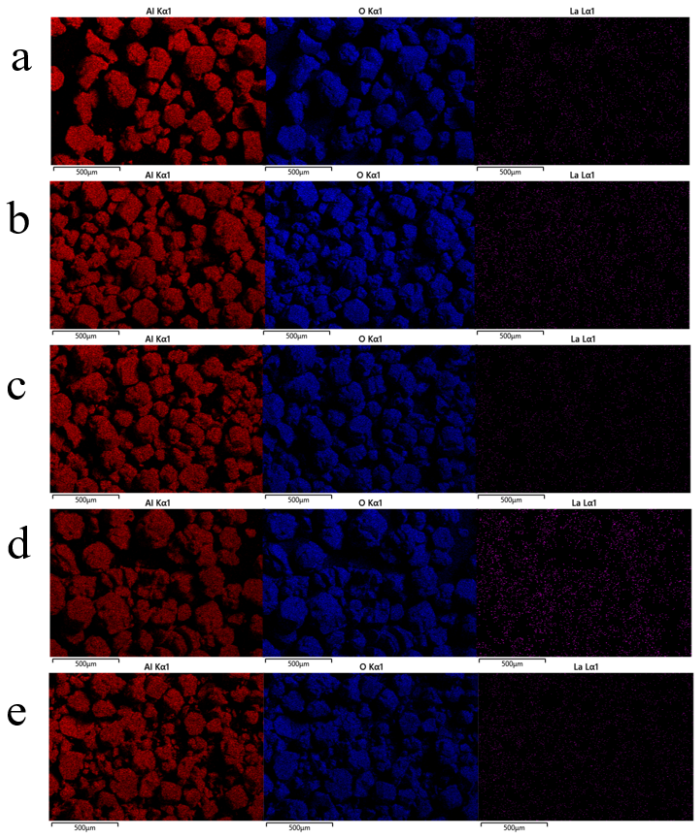

Figure 3. EDS-mapping of samples: (**a**) 2.5% La-AA, (**b**) 5% La-AA, (**c**) 7.5% La-AA, (**d**) 10% La-AA, and (**e**) 12.5% La-AA.

The N_2 adsorption-desorption isotherms (Figure 4a) for all samples are type IV with H4-type hysteresis loops, characteristic of mesoporous materials with slit-shaped pores [30]. The textural parameters are summarized in Table 2. Alkali pretreatment (NaOH-AA) increased the BET surface area and total pore volume compared to pristine AA, likely due to the partial dissolution of amorphous alumina, enlarging some micropores into mesopores. Critically, upon La loading, a systematic decrease in BET surface area (from 180.3 to 168.4 $m^2 \cdot g^{-1}$) and total pore volume was observed. Meanwhile, as La loading rose, the micropore surface area of the samples increased steadily, accompanied by a decline in pore volume (Figure 4b). This trend suggests that La species were initially deposited within mesopores and potentially on the external surface, leading to partial pore blockage or narrowing, which is consistent with the successful incorporation of the modifier.

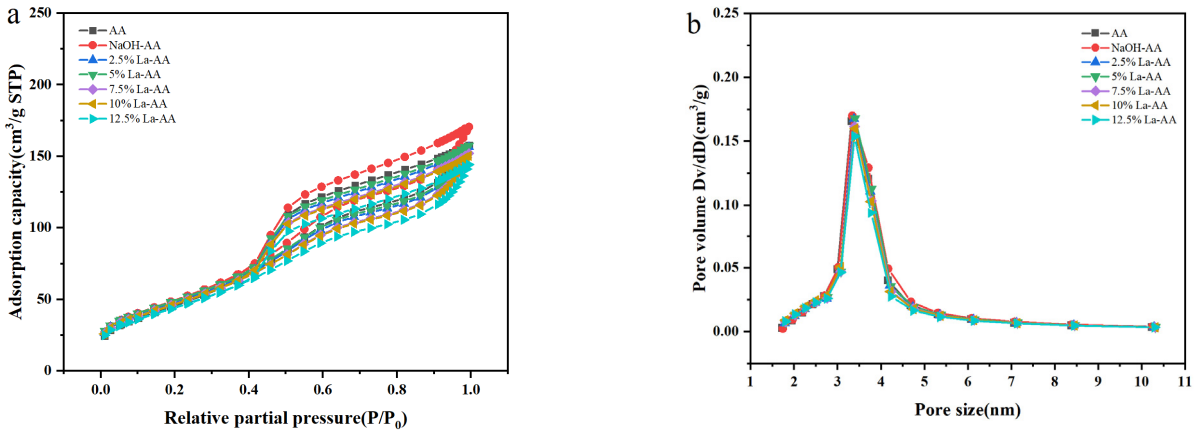

Figure 4. BET analysis: (**a**) N_2 adsorption−desorption isotherm and (**b**) Pore size distribution.

Table 2. Textural properties of the adsorbents.

Samples	BET Specific Surface Area ($m^2 \cdot g^{-1}$)	Total Pore Volume ($cm^3 \cdot g^{-1}$)	Micropore Volume ($cm^3 \cdot g^{-1}$)	Micropore Area ($m^2 \cdot g^{-1}$)	Average Pore Size (nm)
AA	179.0621	0.2438	0.0474	29.6435	4.1938
NaOH-AA	191.4477	0.2638	0.0426	21.6999	4.3264
2.5% La-AA	180.3236	0.2422	0.0543	45.6308	4.3368
5% La-AA	178.7158	0.2401	0.0569	49.0223	4.3158
7.5% La-AA	175.6099	0.2351	0.0564	50.9298	4.3323
10% La-AA	172.7627	0.2325	0.0564	53.5293	4.2915
12.5% La-AA	168.3990	0.2231	0.0559	55.2019	4.3507

The chemical compositions of the 10% LA-AA before and after fluorine absorption were characterized by XPS. As shown in Figure 5a, the core-levels like C 1s, O 1s, Al 2p, La 3d, and F 1s can be identified. The detailed oxidation states of the 10% LA-AA before and after fluorine absorption were revealed in high resolution XPS. The high-resolution XPS spectrum of C 1s (Figure 5b) for the sample before and after fluorine adsorption can be divided into three main peaks near 284.8, 286.4, and 289.0 eV, assigned to C–C, C–O, and C=O, respectively [31]. As shown in Figure 5c, the O 1s spectrum for the sample before and after fluorine adsorption can be divided into three peaks near 530.6, 531.6, and 533.0 eV, which were attributed to surface lattice oxygen (M–O, M = La or Al), surface hydroxyl (-OH), and chemically or physically adsorbed water (H_2O), respectively [32,33].

It is worth noting that after fluorine adsorption, the intensity of the -OH peak on O 1s decreases, indicating that F has replaced some -OH groups. In the Al 2p spectrum before fluorine absorption (Figure 5d), only one peak observed at 74.7 eV corresponded to aluminum atoms binding with oxygen (Al–O) in the adsorbent. After fluorine adsorption, a new peak observed at 75.5 eV corresponds to Al–F in the adsorbent. Figure 5e displays the high-resolution spectra of La3d before and after fluorine adsorption for 10% La-AA. The La3d spectrum comprises two peaks, each of which can be divided into paired intensity peaks. Before adsorption, the two main peaks, La3d5/2 and La3d3/2, are located at 835.7 and 852.5 eV, respectively, with their corresponding satellite peaks at 839.2 eV and 856.1 eV, respectively. This indicates the presence of La–O. After fluorine adsorption, the binding energies of La 3d5/2 and La3 d3/2 shift to higher energy values, becoming 836.8 and 853.5 eV, respectively, with their corresponding satellite peaks at 840.8 eV and 857.5 eV, respectively. This may be attributed to the formation of La–F. The F 1s spectrum after fluorine adsorption (Figure 5f) exhibits two characteristic peaks at 685.0 and 687.8 eV, which can be attributed to the fluoride metal complexes M–F and fluoride metal coatings (MFn), respectively [34].

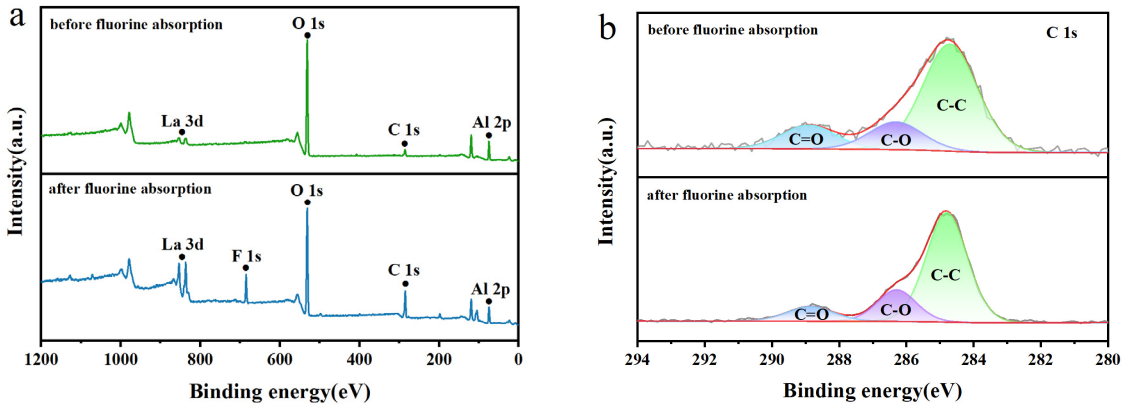

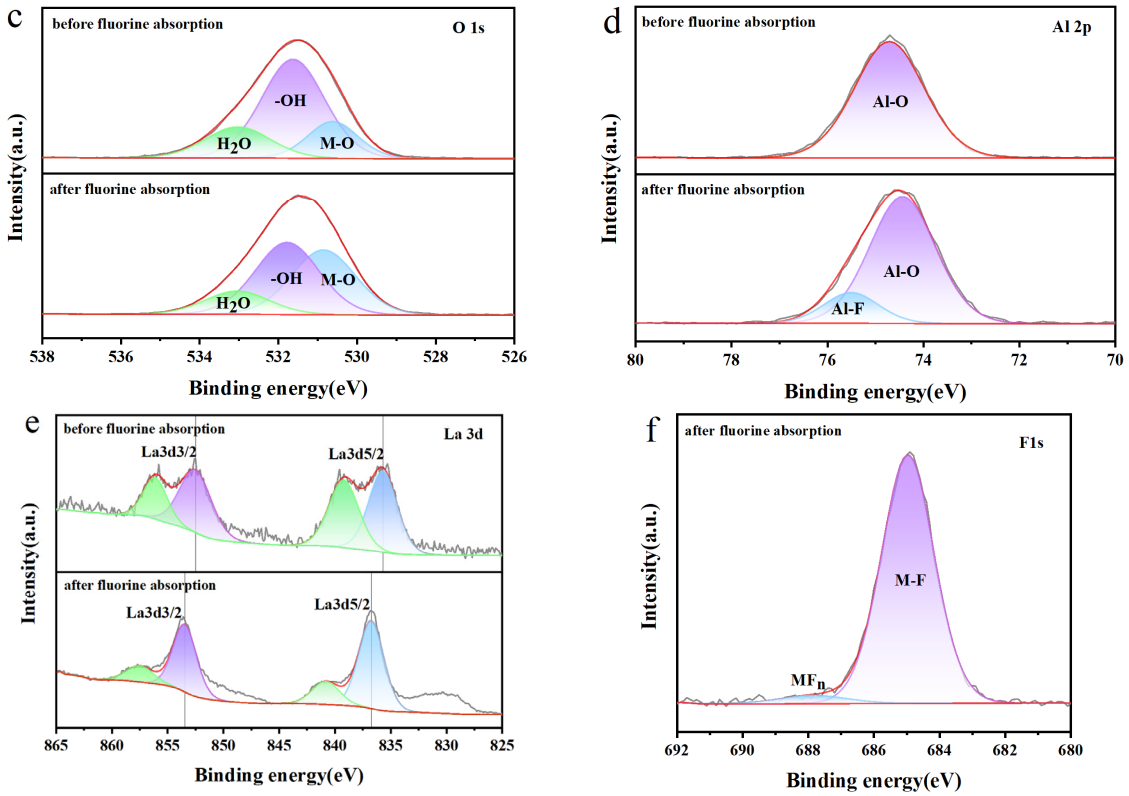

Figure 5. XPS spectra of the 10%LA-AA before and after fluorine absorption: (**a**) full range spectrum; and high-resolution of (**b**) C 1s; (**c**) O 1s; (**d**) Al 2p; (**e**) La 3d; (**f**) F 1s.

3.2. Adsorption Performance and Mechanism Exploration

We first evaluated the adsorption performance by investigating the effects of several key parameters. La doping was the decisive factor for performance enhancement. As shown in Figure 6a, the fluoride adsorption capacity increased non-linearly as the La loading rose. At 0% La doping (pristine AA), the adsorption capacity reaches 2.23 mg/g (under non optimal adsorption conditions), attributed to conventional mechanisms including ion exchange ($OH^- \rightarrow F^-$) and electrostatic attraction at Al^{3+} sites. After lanthanum modification, the fluoride adsorption capacity of the adsorbent increased significantly. The potential reasons are presented as follows: 1. The main chemical pathway for fluoride removal was ligand exchange between surface hydroxyl groups and fluoride ions. After La modification, abundant ≡La–OH active sites formed on the adsorbent surface. The hydroxyl groups bonded to high-valence La^{3+} were highly active and readily exchanged with F^- in solution to generate stable ≡La–F complexes. Compared with pristine Al–OH sites on raw alumina, La–OH exhibited much stronger affinity toward fluoride. 2. Weak electrostatic attraction served as an auxiliary adsorption mechanism. The surface of La-modified samples carried more positive charges, which facilitated the capture of anionic F^- through electrostatic interaction. 3. Combined with XPS characterization results, the new characteristic peak of La–F after fluoride adsorption directly verified the formation of chemical bonding between lanthanum species and fluoride ions. The adsorption capacity of 10% La-AA reached 9.49 $mg \cdot g^{-1}$, which was 4.3 times that of the pristine AA (2.23 $mg \cdot g^{-1}$). When the La loading was further increased to 12.5%, the fluoride adsorption capacity only climbed to 9.80 $mg \cdot g^{-1}$. The above fluoride adsorption behavior originates from two factors at 12.5% nominal La loading: the slight rise in actual lanthanum loading (Table 1) and the decreased pore volume and surface area of the adsorbent (Figure 4 and Table 2). The 10% La-AA sample achieved optimal cost-effectiveness for fluoride removal, exhibiting excellent adsorption capacity while reducing lanthanum consumption. Therefore, 10% lanthanum doping was set as the optimum condition.

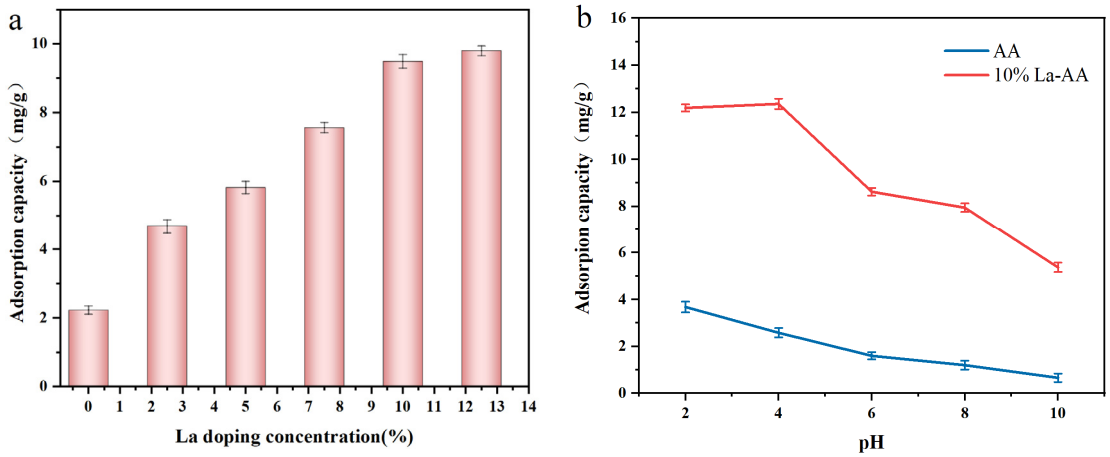

Figure 6. Key factors influencing fluoride adsorption on AA and 10% La−AA: (**a**) Effect of La loading; (**b**) Effect of solution pH.

Solution pH critically regulates adsorption by modulating surface charge and fluoride speciation. The capacity of pristine AA decreased monotonically across the pH 2–10 range, performing poorly under strong acidity (Figure 6b). In stark contrast, 10% La-AA exhibited a pronounced adsorption maximum at pH 4 (12.36 mg·g^{-1}) and maintained superior performance in the acidic range (pH 2–6). This distinct behavior strongly indicates that La^{3+} incorporation creates highly stable and active specific sites that operate effectively under acidic conditions, a key advantage for treating acidic phosphogypsum leachate. Performance declined under alkaline conditions (pH > 8) for both materials due to surface deprotonation and OH^- competition.

The optimization of other operational parameters is also conducted. In the adsorbent dosage range of 0.05–0.25 g, the adsorption capacity per unit mass decreased with increasing dosage (Figure S1), attributable to site underutilization at low solute-to-site ratios. A dosage of 0.05 g was selected for subsequent mechanistic studies to maximize capacity data. The adsorption capacity increased with higher initial F^- concentration (25–300 mg·L^{-1}), driven by a stronger concentration gradient, forming the basis for the isotherm studies (Figure S2). Within the reaction temperature range of 25–85 °C, the fluoride ion adsorption capacity of 10% La-AA first increases and then decreases, reaching its peak at 70 °C (Figure S3). In contrast, the fluoride ion adsorption capacity of AA gradually increases. Adsorption equilibrium for both materials was achieved within 60 min (Figure S4). Hence, a 1-h contact time was adopted for all batch experiments.

The dramatic performance enhancement prompted a systematic investigation into the underlying adsorption mechanism. We employed kinetic, isotherm, and thermodynamic analyses to compare AA and 10% La-AA, aiming to understand how La doping fundamentally governs the adsorption process.

Adsorption kinetics (Figure 7 and Table 3) revealed not only a large increase in equilibrium capacity (q_e: 2.90 to 10.05 mg·g^{-1}) but, more importantly, a change in the governing kinetic model. The adsorption on pristine AA was best described by the pseudo-first-order (PFO) model (R^2 = 0.9743), indicative of a process potentially limited by physical diffusion to the surface. In stark contrast, adsorption on 10% La-AA was best fitted by the pseudo-second-order (PSO) model (R^2 = 0.9830). The PSO model is typically associated with chemisorption, where the rate is proportional to the square of the number of available sites, suggesting that surface chemical reaction, suggesting that electron transfer, or covalent bond formation between the adsorbate and La sites, becomes the new rate-limiting step after La doping. The PSO rate constant (K_2) decreased from 2.4166 for AA to 1.4516, indicating that La doping slightly slowed the initial adsorption rate, likely due to increased surface complexity and potential pore blockage effects.

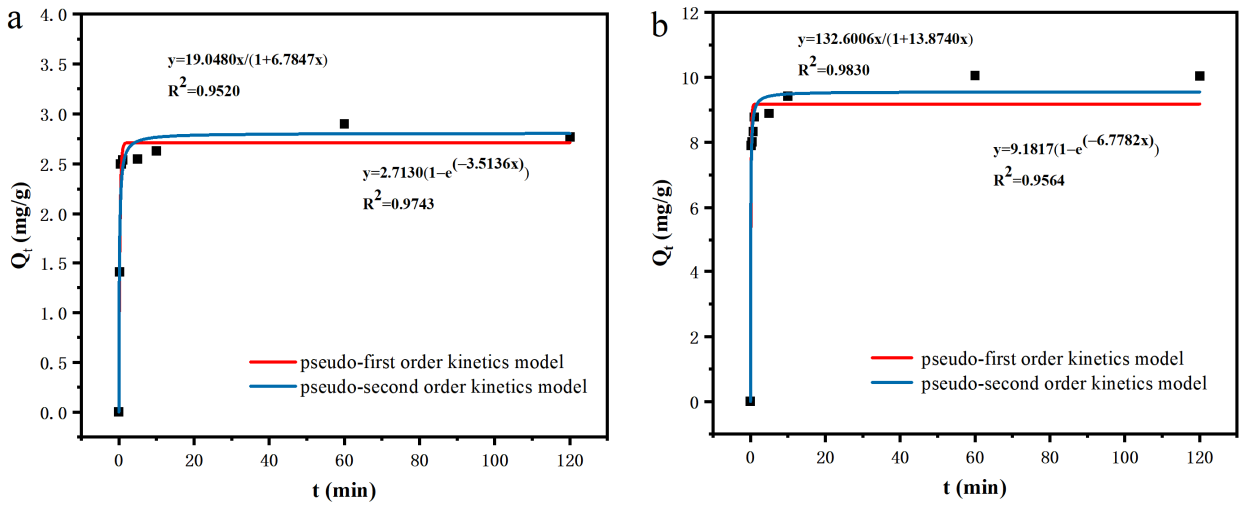

Figure 7. Adsorption kinetics and model fitting: (**a**) AA; (**b**) 10% La-AA.

Table 3. Adsorption kinetic parameters of AA and 10% La-AA.

Samples	Models						
	Adsorption Capacity	Pseudo-First-Order Kinetic			Pseudo-Second Order Kinetic		
	q_e (mg·g^{-1})	K_1	R^2	S	K_2	R^2	S
AA	2.90	3.5136	0.9743	2.71	2.4166	0.9520	2.80
10% La-AA	10.05	6.7782	0.9564	9.18	1.4516	0.9830	9.55

Adsorption isotherms (Figure 8) were analyzed to understand capacity and surface heterogeneity. For both materials, the Freundlich model provided a superior fit over the Langmuir model (Table 4), indicating multilayer adsorption on heterogeneous surfaces [29,35]. The key parameters, however, differed profoundly. The Freundlich intensity parameter n increased from ~1.1 (AA) to ~3.0 (La-AA), signifying a much more favorable adsorption process and stronger adsorbate-adsorbent interaction [36]. The capacity constant K_F increased by several orders of magnitude, quantitatively capturing the massive enhancement.

Table 4. Adsorption isotherm model parameters of AA and 10% La-AA.

Sample	Model	Langmuir Isotherm Model			Freundlich Isotherm Model		
	T (K)	q_{max} (mg·g^{-1})	K_L (L·mg^{-1})	R^2	K_F (mg/g(L/mg)$^{1/n}$)	n	R^2
AA	298	100	0.0005	0.0260	0.0018	1.0712	0.9861
	308	30.395	0.0022	0.2445	0.0050	1.1587	0.9845
	318	18.5874	0.0036	0.1465	0.0034	1.1380	0.9791
10% La-AA	298	25.1256	0.0262	0.9746	17.9019	2.9603	0.9903
	308	29.1545	0.0186	0.9504	16.5615	2.8425	0.9769
	318	22.7273	0.0326	0.9136	26.7239	3.4317	0.9549

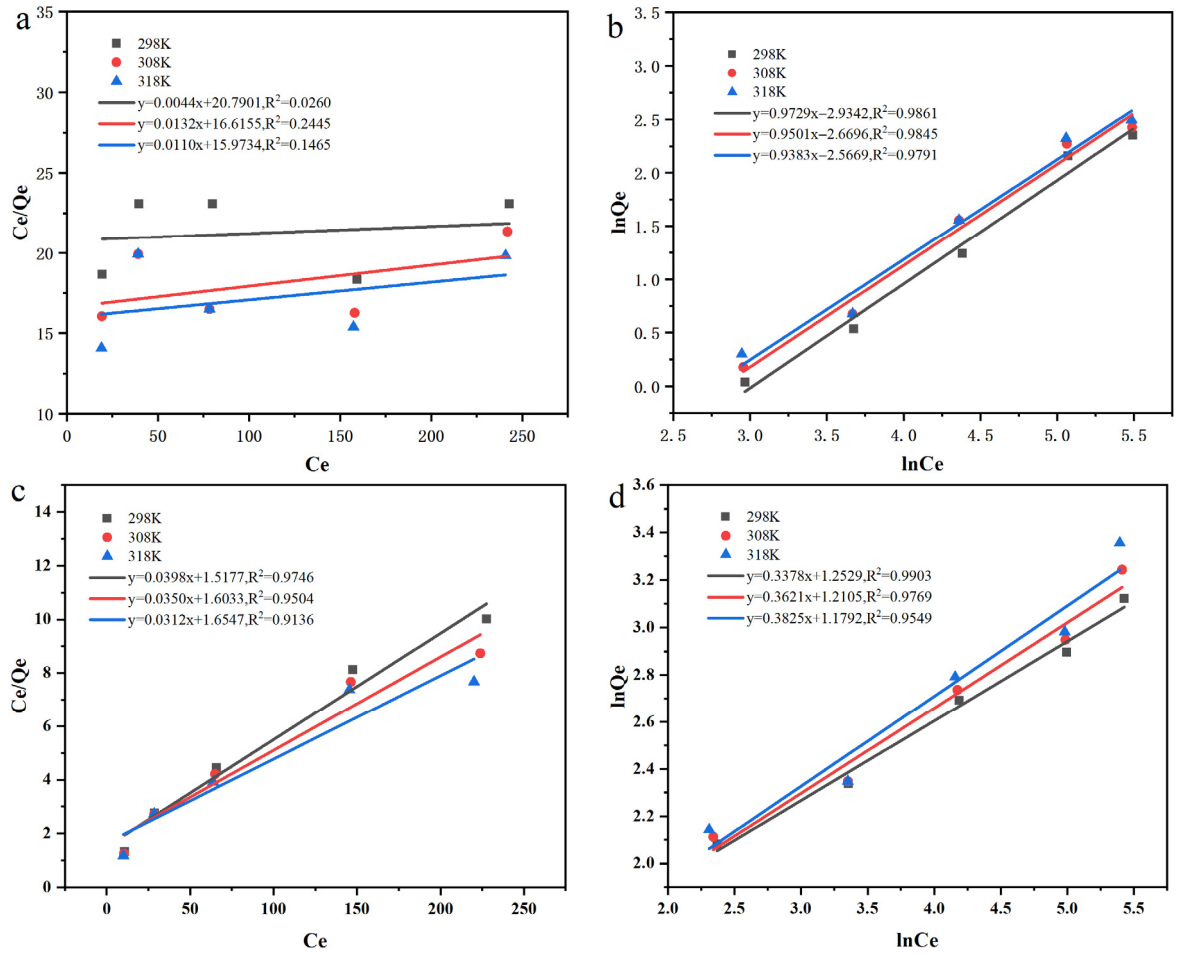

Figure 8. Adsorption isotherms and model fitting: (**a**) AA of Langmuir; (**b**) AA of Freundlich; (**c**) 10% La-AA of Langmuir; (**d**) 10% La-AA of Freundlich.

Thermodynamic parameters (Figure 9 and Table 5) provided pivotal energetic insights [37]. For AA, the positive ΔG^0 values (7.25 to 6.99 KJ·mol^{-1}) indicated a non-spontaneous adsorption process under the studied conditions, with a positive ΔH^0 (11.13 KJ·mol^{-1}) confirming its endothermic nature. For 10% La-AA, the ΔG^0 values dropped remarkably to near zero (0.72 to 0.44 KJ·mol^{-1}), signaling that the process approaches spontaneity. The significantly lower ΔH^0 (4.79 KJ·mol^{-1}) indicates a reduced energy barrier for adsorption on La-AA.

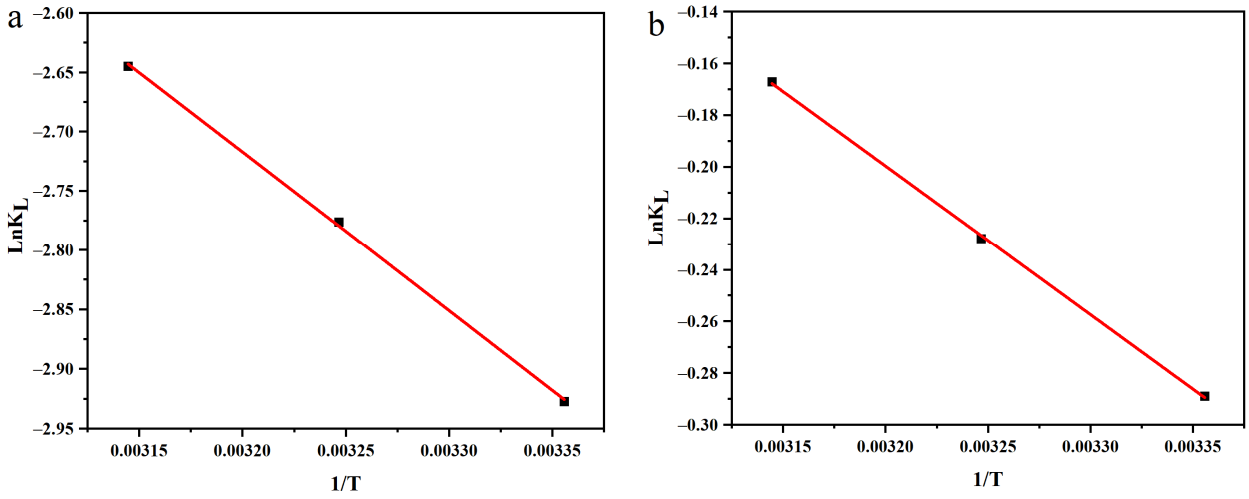

Figure 9. Linear regression of the thermodynamics of F^- adsorption of (**a**) AA; (**b**) 10% La-AA.

Table 5. Thermodynamic parameters of adsorption onto AA and 10% La-AA at different temperatures.

Sample	T (K)	lnK_L	R^2	ΔG (KJ·mol^{-1})	ΔS (J·(mol·K)$^{-1}$)	ΔH (KJ·mol^{-1})
AA	298	−2.9274	0.9995	7.2527	13.0372	11.1333
	308	−2.7762		7.1090		
	318	−2.6448		6.9926		
10% La-AA	298	−0.2889	0.9997	0.7158	13.6815	4.7945
	308	−0.2279		0.5836		
	318	−0.1672		0.4420		

The convergent evidence from kinetics, isotherms, and thermodynamics conclusively shows that La^{3+} acts as a stronger Lewis acid site compared to Al^{3+}. Fluoride ions (a hard Lewis base) form stronger inner-sphere complexes with these La sites (La–F bonds). This is manifested as: (i) a kinetics shift to chemisorption control, (ii) a massive increase in adsorption affinity (n) and capacity (K_F), and (iii) a favorable shift in thermodynamic spontaneity and enthalpy. La doping thus fundamentally re-engineers the adsorption interface, introducing qualitatively superior sites with stronger driving forces.

3.3. Selectivity Toward Fluoride in the Presence of Competing Anions

A critical requirement for an adsorbent targeting industrial wastewater is selectivity against competing ions. Phosphogypsum leachate is rich in anions like phosphate and sulfate. As shown in Figure 10, the presence of Cl^-, SO_4^{2-}, and PO_4^{3-} (at a 10:1 molar ratio) inhibited F^- uptake on both adsorbents, with an interference order of $PO_4^{3-} > SO_4^{2-} > Cl^-$, consistent with their charge density and affinity for metal centers [18,38].

The most compelling finding, however, lies in the absolute performance. In the control (F^- only), 10% La-AA's capacity was 5.75 times that of AA. Crucially, even under the strongest interference from PO_4^{3-}, the absolute F^- adsorption capacity of La-AA (1.91 mg·g^{-1}) remained more than double the capacity of pristine AA (0.92 mg·g^{-1}). This result decisively demonstrates that La modification confers not just high capacity, but exceptional selectivity and robustness in complex ionic environments, directly addressing a key limitation of conventional AA.

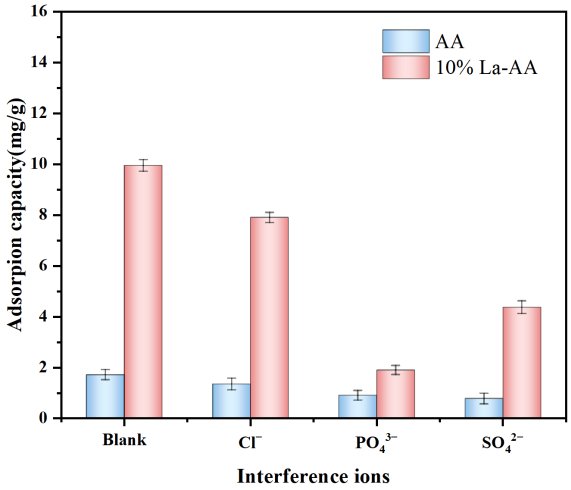

Figure 10. Competitive adsorption effects.

3.4. Application to Authentic Phosphogypsum Leachate

The ultimate test of the developed La-AA adsorbent was its application to real phosphogypsum leachate, characterized by extreme salinity and ultra-high phosphate concentration (Table 6). The leachate was diluted 100-fold to a challenging but relevant F^- concentration of 9.67 mg·L^{-1} for the treatment test.

Table 6. Chemical composition of phosphogypsum leachate.

Ion Species	Mg^{2+}	Ca^{2+}	F^-	SO_4^{2-}	PO_4^{3-}
Concentration ($mg \cdot L^{-1}$)	1326	1160	878	4866	10,949

As shown in Figure 11, 10% La-AA achieved an outstanding 94.0% fluoride removal at an adsorbent dosage of 25 g/L, reducing the F^- concentration to 0.58 $mg \cdot L^{-1}$, which is below the WHO drinking water guideline [36]. This successful decontamination in a matrix containing ~110 $mg \cdot L^{-1}$ of PO_4^{3-} (in the diluted sample) serves as the definitive, real-world validation of the mechanisms proposed above. This phenomenon can be attributed to the competitive displacement adsorption resulting from the varying affinities of the adsorbent for different ions, despite the presence of numerous other ions in the phosphogypsum leachate. When adsorption sites are limited, phosphate ions with higher affinity are preferentially captured by the adsorbent. Subsequently, with the continued addition of the adsorbent, fluoride ions can also be gradually removed [28,39]. It suggests that the strong La–F interaction and the resulting high selectivity are effective even in highly competitive, multi-component industrial wastewater. This result transitions the work from a mechanistic study to a demonstration of significant application potential.

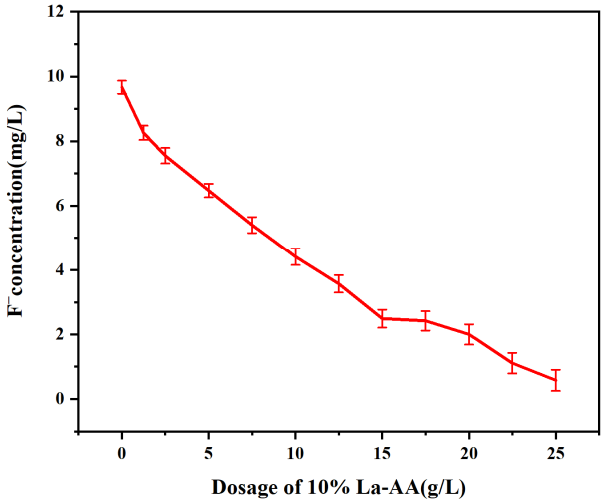

Figure 11. Fluoride removal of 10% La-AA from real phosphogypsum leachate.

4. Conclusions

In this study, lanthanum-modified activated alumina was prepared and evaluated for selective fluoride removal from complex phosphate-industry wastewater. The optimal 10% La loading for fluoride capture was identified. Combined with multiple microscopic characterizations, we clarified that excessive lanthanum species only slightly improve defluoridation performance. We quantitatively revealed the competitive interplay between accessible La active sites and pore structure reduction, providing a sound explanation for the nonlinear growth of fluoride adsorption capacity. Compared with pristine activated alumina, La-AA displays better tolerance to competing anions, especially phosphate, indicating that La modification is effective in enhancing fluoride selectivity under complex matrix conditions. Kinetic and thermodynamic analyses suggest that fluoride adsorption on La-AA is more favorable and the process approaches spontaneity under the tested conditions. Importantly, the optimized La-AA successfully reduced fluoride concentration in authentic phosphogypsum leachate from 9.67 $mg \cdot L^{-1}$ to 0.58 $mg \cdot L^{-1}$, demonstrating its practical potential for fluoride control in phosphate-related industrial process water. This adsorbent is synthesized via a facile impregnation route using low-cost commercial activated alumina as the raw material, thereby greatly enhancing its prospects for large-scale industrial application. Overall, this work provides both mechanistic understanding and application-oriented evidence for the use of La-

modified activated alumina in the selective removal of fluoride from challenging industrial effluents. Further studies on regeneration, long-term stability, and continuous-flow operation would be valuable for assessing its industrial applicability.

Supplementary Materials

The following supporting information can be found at: https://www.sciepublish.com/article/pii/1132, Figure S1: Effects of dosage of AA and 10% La-AA on the fluoride ion adsorption. Figure S2: Effects of concentration of F^- on the fluoride ion adsorption. Figure S3: Effects of temperature on the fluoride ion adsorption. Figure S4: Effects of adsorption time on the fluoride ion adsorption.

Statement of the Use of Generative AI and AI-Assisted Technologies in the Writing Process

During the preparation of this manuscript, the author(s) used DeepSeek to enhance the accuracy of English writing and detect grammatical errors. After utilizing this tool, the author(s) thoroughly reviewed and revised the full manuscript, verified all scientific data, experimental details and the validity of research conclusions, and take(s) full responsibility for all content of this published paper.

Acknowledgements

The authors would like to thank Shiyanjia Lab (www.shiyanjia.com) for the characterization support.

Author Contributions

Conceptualization, Z.W.; Methodology, S.H. (Shuomin Hou); Investigation, S.H. (Shuomin Hou); Resources, Z.W., S.H. (Shengchao Huang) and H.M.; Data Curation, S.H. (Shuomin Hou) and Z.W.; Writing—Original Draft Preparation, S.H. (Shuomin Hou); Writing—Review & Editing, Z.W. and X.P.; Visualization, S.H. (Shuomin Hou); Supervision, Z.W. and R.C.; Project Administration, Z.W. and R.C.; Funding Acquisition, Z.W.

Ethics Statement

Not Applicable.

Informed Consent Statement

Not Applicable.

Data Availability Statement

The authors confirm that the data supporting the findings of this study are available within the article and its supplementary materials.

Funding

The authors gratefully acknowledge financial support from the Natural Science Foundation of Hubei Province (Grant Nos. 2025AFD245 and 2025AFD315), the Natural Science Foundation of Yichang Municipality (Grant Nos. A24-3-044 and A25-3-020) , and the Open and Innovation Fund of Hubei Three Gorges Laboratory (Grant Nos. SC250002).

Declaration of Competing Interest

The authors declare that they have no known competing financial interests or personal relationships that could have appeared to influence the work reported in this paper.

References

1. Srivastava S, Flora SJS. Fluoride in Drinking Water and Skeletal Fluorosis: A Review of the Global Impact. *Curr. Environ. Health Rep.* **2020**, *7*, 140–146. DOI:10.1007/s40572-020-00270-9
2. Ghosh A, Mukherjee K, Ghosh SK, Saha B. Sources and Toxicity of Fluoride in the Environment. *Res. Chem. Intermed.* **2013**, *39*, 2881–2915. DOI:10.1007/s11164-012-0841-1
3. Jha SK, Mishra VK, Sharma DK, Damodaran T. Fluoride in the Environment and Its Metabolism in Humans. In *Reviews of Environmental Contamination and Toxicology*; Whitacre DM, Ed.; Springer: New York, NY, USA, 2011; Volume 211, pp. 121–142.
4. He Y, Huang L, Song B, Wu B, Yan L, Deng H, et al. Defluorination by Ion Exchange of SO_4^{2-} on Alumina Surface: Adsorption Mechanism and Kinetics. *Chemosphere* **2021**, *273*, 129678. DOI:10.1016/j.chemosphere.2021.129678
5. You K, Li P, Fu J, Kang N, Gao Y, Cheng X, et al. Fabrication of Manganese-Supported Activated Alumina Adsorbent for Defluoridation of Water: A Kinetics and Thermodynamics Study. *Water* **2021**, *13*, 1219. DOI:10.3390/w13091219
6. Kumari U, Behera SK, Meikap BC. Defluoridation of Synthetic and Industrial Wastewater by Using Acidic Activated Alumina Adsorbent: Characterization and Optimization by Response Surface Methodology. *J. Environ. Sci. Health Part A* **2019**, *54*, 79–88. DOI:10.1080/10934529.2018.1521674
7. Ekamparam ASS, Khaitan H, Nimesh V, Singh A. Relative Extents, Mechanisms, and Kinetics of Fluoride Removal from Synthetic Groundwater by Prevalent Sorbents. *Chemosphere* **2023**, *342*, 140161. DOI:10.1016/j.chemosphere.2023.140161
8. Hiemstra T, Riemsdijk WHV. A Surface Structural Approach to Ion Adsorption: The Charge Distribution (CD) Model. *J. Colloid Interface Sci.* **1996**, *179*, 488–508. DOI:10.1006/jcis.1996.0242
9. Yu C, Liu L, Wang X, Fu J, Wu Y, Feng C, et al. Fluoride Removal Performance of Highly Porous Activated Alumina. *J. Sol-Gel Sci. Technol.* **2023**, *106*, 471–479. DOI:10.1007/s10971-022-05722-2
10. Lin JY, Chen YL, Hong XY, Huang C, Huang CP. The Role of Fluoroaluminate Complexes on The Adsorption of Fluoride onto Hydrous Alumina in Aqueous Solutions. *J. Colloid Interface Sci.* **2020**, *561*, 275–286. DOI:10.1016/j.jcis.2019.10.085
11. Gai WZ, Zhang SH, Yang Y, Sun K, Jia H, Deng ZY. Defluoridation Performance Comparison of Aluminum Hydroxides with Different Crystalline Phases. *Water Supply* **2022**, *22*, 3673–3684. DOI:10.2166/ws.2022.012
12. Xiao J, Sun W, Song Y, Li Q, Wu M, Yang Y. Removal of Fluoride Ions from Zinc Sulfate Solution by Mesoporous Alumina: Performance and Mechanism. *Hydrometallurgy* **2025**, *234*, 106471. DOI:10.1016/j.hydromet.2025.106471
13. Gao S, Cui J, Wei Z. Study on The Fluoride Adsorption of Various Apatite Materials in Aqueous Solution. *J. Fluor. Chem.* **2009**, *130*, 1035–1041. DOI:10.1016/j.jfluchem.2009.09.004
14. Ku Y, Chiou HM. The Adsorption of Fluoride Ion from Aqueous Solution by Activated Alumina. *Water Air Soil Pollut.* **2002**, *133*, 349–361. DOI:10.1023/A:1012929900113
15. Dolganov AV, Balandina AV, Chugunov DB, Timonina AS, Knyazev AV. Sorption of Fluoride Ions onto Cellulose and Aluminum Oxide Composites. *Russ. J. Inorg. Chem.* **2020**, *65*, 1770–1775. DOI:10.1134/s0036023620110030
16. Badillo-Almaraz VE, Solache-Ríos MJ, Badillo-Almaraz V, Zarate-Morales A, Flores-Moreno A. Radiotracer Techniques (^{18}F) and Modeling of Fluoride Sorption on Alumina. *J. Fluor. Chem.* **2017**, *199*, 113–118. DOI:10.1016/j.jfluchem.2017.04.001
17. Kundu S, Chowdhury IH, Sinha PK, Naskar MK. Effect of Organic Acid-Modified Mesoporous Alumina toward Fluoride Ions Removal from Water. *J. Chem. Eng. Data* **2017**, *62*, 2067–2074. DOI:10.1021/acs.jced.7b00129
18. Singh PK, Saharan VK, George S. Studies on Performance Characteristics of Calcium and Magnesium Amended Alumina for Defluoridation of Drinking Water. *J. Environ. Chem. Eng.* **2018**, *6*, 1364–1377. DOI:10.1016/j.jece.2018.01.053
19. Kumari U, Siddiqi H, Bal M, Meikap BC. Calcium and Zirconium Modified Acid Activated Alumina for Adsorptive Removal of Fluoride: Performance Evaluation, Kinetics, Isotherm, Characterization and Industrial Wastewater Treatment. *Adv. Powder Technol.* **2020**, *31*, 2045–2060. DOI:10.1016/j.apt.2020.02.035
20. Sanini B, Leichtweis J, Silvestri S, Welter N, Emiliano C, Mancuso MA, et al. Impregnation of Activated Alumina with CeO_2 for Water Defluoridation. *Mater. Chem. Phys.* **2022**, *291*, 126648. DOI:10.1016/j.matchemphys.2022.126648
21. Duan Y, Wang C, Li X, Xu W. Fluoride Adsorption Properties of Three Modified Forms of Activated Alumina in Drinking Water. *J. Water Health* **2014**, *12*, 715–721. DOI:10.2166/wh.2014.016
22. Luo Z, Zhang J, Liu Z, Tang K, Zhang D, Hou Y, et al. Performance and Mechanism of Manganese-modified Activated Alumina for Cost-Effective Removal of Fluorine from Water. *Mater. Today Commun.* **2025**, *48*, 113555. DOI:10.1016/j.mtcomm.2025.113555
23. Saraiva ÍCG, Ezaki S, Calabria GD, Shinzato MC. Groundwater Defluoridation Efficacy of Manganese-Oxide-Coated Alumina Prepared via Two-Step Heating. *Environ. Technol.* **2022**, *43*, 2684–2696. DOI:10.1080/09593330.2021.1894242

24. Zhu X, Wen B, Fan C, Zhang L. The Discovering of Rapid Formation $La(OH)_3$ from LaH_3. *Green Chem. Technol.* **2024**, *1*, 10005. DOI: 10.70322/gct.2024.10005
25. Zhang Y, Lin X, Zhou Q, Luo X. Fluoride Adsorption from Aqueous Solution by Magnetic Core-Shell Fe_3O_4@Alginate-La Particles Fabricated via Electro-Coextrusion. *Appl. Surf. Sci.* **2016**, *389*, 34–45. DOI:10.1016/j.apsusc.2016.07.087
26. He Y, Zhang L, An X, Wan G, Zhu W, Luo Y. Enhanced Fluoride Removal from Water by Rare Earth (La and Ce) Modified Alumina: Adsorption Isotherms, Kinetics, Thermodynamics and Mechanism. *Sci. Total Environ.* **2019**, *688*, 184–198. DOI:10.1016/j.scitotenv.2019.06.175
27. Jiang S, Wang Z, Qin Y, Cao B, Chi R. Eco-Friendly Synthesis of Spherical Lanthanum-Doped Hydroxyapatite from Phosphogypsum Waste: A High-Efficiency Strategy for Fluoride Removal in Aqueous Solutions. *Green Chem. Technol.* **2026**, *3*, 10008. DOI: 10.70322/gct.2026.10008
28. Zhao M, Zhou X, Li J, Li F, Li X, Yu J, et al. Efficient Removal of Phosphate and Fluoride from Phosphogypsum Leachate by Lanthanum-Modified Zeolite: Synchronous Adsorption Behavior and Mechanism. *J. Environ. Chem. Eng.* **2024**, *12*, 113294. DOI:10.1016/j.jece.2024.113294
29. Dhawane SH, Khan AA, Singh K, Tripathi A, Hasda R, Halder G. Insight into Optimization, Isotherm, Kinetics, and Thermodynamics of Fluoride Adsorption onto Activated Alumina. *Environ. Prog. Sustain. Energy* **2017**, *37*, 766–776. DOI:10.1002/ep.12814
30. Sing K. The Use of Nitrogen Adsorption for The Characterisation of Porous Materials. *Colloid Surface A* **2001**, *187–188*, 3–9. DOI:10.1016/S0927-7757(01)00612-4
31. Kang D, Yu X, Ge M, Lin M, Yang X, Jing Y. Insights into adsorption mechanism for fluoride on cactus-like amorphous alumina oxide microspheres. *Chem. Eng. J.* **2018**, *345*, 252–259. DOI:10.1016/j.cej.2018.03.174
32. Yu X, Kang D, Hu Y, Tong S, Ge M, Cao C, et al. One-pot synthesis of porous magnetic cellulose beads for the removal of metal ions. *RSC Adv.* **2014**, *4*, 31362. DOI:10.1039/c4ra05601a
33. Ekka B, Dhaka RS, Patel RK, Dash P. Fluoride removal in waters using ionic liquid-functionalized alumina as a novel adsorbent. *J. Clean. Prod.* **2017**, *151*, 303–318. DOI:10.1016/j.jclepro.2017.03.061
34. Sun X, Ke C, Lu Q, Liang L, Xie G. Adsorption of fluoride ion on Al/La modified acidified attapulgite composite materials. *Sep. Purif. Technol.* **2025**, *354*, 128791. DOI:10.1016/j.seppur.2024.128791
35. Xiang B, Tang J, Feng X, Zhu Y, Li Y, Tan T. Preparation of Aluminium-Hydroxide-Modified Diatomite and Its Fluoride Adsorption Mechanism. *Sci. Rep.* **2023**, *13*, 3871. DOI:10.1038/s41598-023-30901-8
36. Chinnakoti P, Chunduri ALA, Vankayala RK, Patnaik S, Kamisetti V. Enhanced Fluoride Adsorption by Nano Crystalline γ-Alumina: Adsorption Kinetics, Isotherm Modeling and Thermodynamic Studies. *Appl. Water Sci.* **2017**, *7*, 2413–2423. DOI:10.1007/s13201-016-0490-9
37. Lima ÉC, Adebayo MA, Machado FM. Kinetic and Equilibrium Models of Adsorption. In *Carbon Nanomaterials as Adsorbents for Environmental and Biological Applications*; Bergmann CP, Machado FM, Eds.; Springer: Cham, Switzerland, 2015; pp. 33–69.
38. Tao W, Zhong H, Pan X, Wang P, Wang H, Huang L. Removal of Fluoride from Wastewater Solution Using Ce-AlOOH with Oxalic Acid as Modification. *J. Hazard. Mater.* **2020**, *384*, 121373. DOI:10.1016/j.jhazmat.2019.121373
39. Xiong WL, Zhang J, Yu JX, Chi RA. Competitive Adsorption Behavior and Mechanism for Pb^{2+} Selective Removal from Aqueous Solution on Phosphoric Acid Modified Sugarcane Bagasse Fixed-Bed Column. *Process Saf. Environ.* **2019**, *124*, 75–83. DOI:10.1016/j.psep.2019.02.001